Bradycardic mice undergo effective heart rate improvement after specific homing to the sino-atrial node and differentiation of adult muscle derived stem cells

Pietro Mesirca, Daria Mamaeva, Isabelle Bidaud, Romain Davaze, Mattia L Difrancesco, Violeta Mitutsova, Angelo Torrente, Nikola Arsic, Joël Nargeot, Jörg Striessnig, et al.

Bradycardic mice undergo effective heart rate improvement after specific homing to the sino-atrial node and differentiation of adult muscle derived stem cells.

Pietro Mesirca[1,2*], Daria Mamaeva[3,8*], Isabelle Bidaud[1,2], Romain Davaze[3,4], Mattia L. DiFrancesco[1-3], Violeta Mitutsova[3,4], Angelo G. Torrente[1,2], Nikola Arsic[3,7], Joël Nargeot[1,2], Jörg Striessnig[5], Amy Lee[6], Ned J. Lamb[3], Matteo E. Mangoni[1,2@] and Anne Fernandez[3@]

[1]Institut de Génomique Fonctionnelle, Département de Physiologie, CNRS, INSERM, Université de Montpellier, 141 rue de la Cardonille, Montpellier, F-34094, France

[2]LabEx Ion Channels Science and Therapeutics (ICST).

[3]Cell Biology group, Institut de Génétique Humaine, CNRS and Université de Montpellier, 141 rue de la Cardonille, Montpellier, F-34396, France.

[4]Université de Montpellier, UM, Montpellier, F-34094, France.

[5]Department of Pharmacology and Toxicology, Institute of Pharmacy, Center for Molecular Biosciences, University of Innsbruck, Austria.

[6]Department of Molecular Physiology and Biophysics, University of Iowa, IA, USA.

[7]present address: Centre de Recherche en Biologie Cellulaire de Montpellier, CNRS, UMR5237, 1919 route de Mende, 34293 Montpellier Cedex 5, France.

[8]present address: Institute for Neurosciences of Montpellier, INSERM U1051, 80 avenue Augustin Fliche, Montpellier, F-34091, France.

* These authors contributed equally to this work

@ authors for correspondence

Abstract

Current treatment for heart automaticity disorders still lack a safe and efficient source of stem cells to bring about biological pacemaking. Since adult Muscle-Derived Stem Cells (MDSC) show multi-lineage differentiation *in vitro* including into spontaneously beating cardiomyocytes, we questioned whether MDSCs could effectively differentiate into cardiac pacemakers, a specific population of myocytes producing electrical impulses in the sino-atrial node of adult heart. We show here that beating cardiomyocytes, differentiated from MDSC *in vitro,* exhibit typical characteristics of cardiac pacemakers: the expression of Hcn4, Tbx3 and Islet1, as well as spontaneous calcium transients and hyperpolarization-activated "funny" current, a unique signature of sino-atrial pacemakers. Pacemaker-like myocytes differentiated *in vitro* from $Ca_v1.3$ -deficient mouse MDSC produced slower Ca^{2+} transients, consistent with the reduction of native pacemaker activity in these mice. In vivo, systemic injection of undifferentiated wild type MDSCs into bradycardic mutant $Ca_v1.3^{-/-}$ mice was ensued by their migration and homing to the sino-atrial node area within 48h and differentiation into $Ca_v1.3$ -expressing pacemaker-like myocytes within 10 days, a process accompanied by a significant improvement of the heart rate after 10 days that was maintained for up to 5 weeks. These findings identify MDSCs as directly transplantable stem cells that efficiently engraft, differentiate and improve heart rhythm in a mouse model of congenital bradycardia.

Introduction

Stem cells with the capacity to self-renew and differentiate into several lineages can be isolated from most adult tissues and organs. However, as the largest vascularised and innervated organ in the body, and one with the life-long ability to undergo atrophy and regeneration, skeletal muscle is particularly rich in multipotent stem cells (reviewed by Peault et al., [1] and by Tamaki et al [2,3]). Various populations of stem cells were isolated from muscle, the best studied being satellite cells. Named from their tight association to muscle fibres, satellite cells account for muscle fibre regeneration and are an heterogeneous population (reviewed by Yin et al. [4]). In addition skeletal muscle contains connective tissue-, vascularisation-, and innervation-derived progenitor and stem cells, which cooperate with satellite cells in tissue repair (reviewed by Peault et al. [1], Tamaki et al. [3] and Ten Broek et al. [5]). Consistent with the neuro-muscular identity of skeletal muscle, differentiation of muscle-derived stem cells into different meso-ectodermal cell lineages was reported in several studies including from human muscle [6-8] and after clonal growth of muscle stem cells [9].

We previously reported that a population of muscle-derived stem cells (MDSCs) [10] isolated from adult mouse muscle on the basis of their low adherence by sequential preplating [11,12] is multipotent [10]. In particular this population spontaneously differentiated into autonomously beating cardiomyocyte-like cells [10]. This autonomous phenotype questioned whether beating cardiomyocytes derived from MDSC may be identical to pacemaker myocytes, a small population of highly specialized cells in the right atrium of adult hearts located in the Sino-Atrial (SAN) and Atrio-Ventricular Node (AVN)[13]. Pacemaker cells are endowed with automatic electrical activity, and this enables them to generate the cardiac impulse that is conducted through the atrial tissue and the AVN, to the Purkinje fibre network from which it depolarizes the ventricular myocardium[13]. In vertebrates, automaticity is one of the first features of cardiogenesis, with all cardiac cells of the early embryo capable of autonomous beating. During late development of the chambers and conduction system, the SAN emerges from a morphologically distinct area that develops within the sinus venosus, at the site where the right atrium enters the intercaval region, due to up-regulation of the Tbx18 and Tbx3 transcription factors and their repression of cardiogenic Nkx2.5[14,15]. The generation and conduction of the pacemaker impulse within the SAN differs from that in working atrial myocytes in that membrane depolarisation is spontaneous and intercellular electrical resistance is high [16,17]. To fulfil this requirement, pacemaker myocytes uniquely express a particular set of ion channels: the hyperpolarisation-activated cAMP-gated cation channel 4, HCN4; voltage-gated $Ca_v1.3$ channels; and a specific subset of connexins, including connexin45 (Cx45) and Cx30.2 (but not the high-conductance gap junction proteins Cx40 and Cx43 which are typically expressed

in working cardiomyocytes) [18,19]. Pacemaker myocytes thus represent a specialized cardiac myocyte type that is essential for proper heart function and whose properties and defining markers are distinct from those of working cardiomyocytes.

In humans, SAN dysfunction (SND) results in reduced life expectancy and necessitates the implantation of >450,000 pacemakers/year in Europe and the U.S., a number predicted to double over the next half century [20]. Whereas pacemaker implantation remains the primary therapy for SAN dysfunction and bradycardia-associated arrhythmias [21], this approach is costly, requiring lifelong management including regular technical inspections. These limitations and complexity in the use of an electronic device are even greater in pediatric and young patients [22]. Considering the global impact of SAN dysfunction, it is generally agreed that new therapeutic strategies are needed. The development of a cell-therapy approach to repair the damaged SAN and restore pacemaker activity is paramount to achieving stable, life-long improved heart function and to restoring patient quality of life [22]. Toward this goal it will be necessary to identify suitable sources of transplantable stem cells that are capable of differentiating, *in vivo*, into functional pacemaker myocytes.

In the current study, we tested the ability of MDSCs to differentiate, both *in vitro* and *in vivo* in mutant mice, into pacemaker myocytes. We report that MDSC can migrate and home to the SAN where they differentiate into pacemaker-like cardiomyocytes, and that this homing and differentiation of MDSCs ameliorates heart rhythm in congenitally bradycardic mutant mice.

Results

In vitro analysis: MDSCs spontaneously differentiate into autonomously beating cardiomyocytes with the characteristics of pacemaker cells.

MDSCs were isolated from mouse hind-limb muscle via sequential preplating of non-adherent cells, as shown in Fig. 1a and described previously [10]. Non-adherent stem cells were replated in fresh proliferation medium every 24 hours to avoid their premature differentiation and to stimulate their proliferation. The rationale for daily replating and centrifugation is two-fold: the replating prevents loss of the less adherent stem cells, which would otherwise attach to counterparts that adhere and proliferate more rapidly (e.g., fibroblasts, myofibroblasts and pre-adipocytes); and the centrifugation depletes the cultures of muscle fibre-derived microsomes and other muscle-specific non-cellular components that may contribute to the myogenic commitment of muscle stem cells. A comparative analysis of the transcriptomes of muscle cells extracted 24 hours after activation of proliferation (corresponding to PP1) and MDSCs isolated after 7 days of pre-plating (corresponding to PP8) revealed a 12-fold increase in cyclinA2 expression (Fig.1b), indicating a high level of cell proliferation. The same analysis revealed a 10-fold increase in the expression of Islet-1, a LIM-homeodomain transcription factor expressed in heart and pancreatic progenitor/stem cells, and a

>30-fold increase in expression of Peg3/PW1, which is expressed in stem cells isolated from muscle and several adult tissues [23]. Of note, the stemness factor Nestin, whose expression is high even in PP1 cells, was increased >2-fold in PP8 MDSCs (Fig. 1b). These data confirm that 7 days of preplating non-adherent cells from mouse skeletal muscle is an effective means of isolating a proliferating stem cell population.

We previously reported that non-adherent MDSCs in PP8 cultures provided with an attachment matrix such as laminin, fibronectin, or a fibroblast layer (but not collagen) became adherent and underwent multi-lineage differentiation [10]. Amongst the different phenotypes observed, cells with the ability to beat autonomously were observed within 3 to 5 days and these cells exhibited persistent contractile activity for over 2 months in culture (Fig.1c and Supplementary video 1). Single beating cells or clusters of cells with coordinated beating rhythms were observed (Supplementary videos 2 and 3), and the morphology of these beating myocytes was reminiscent of that of native SAN pacemaker cells (Supplementary Fig. 1). Henceforth, we refer to these *in vitro* differentiated, spontaneously beating cells as MDSC-derived pacemaker-like cells (MDSC-PMs). To investigate whether these cells exhibit properties of SAN cardiomyocytes, we first analyzed a number of molecular markers of pacemaker development and activity. SAN development is initiated in a small area of the septum venosus that co-expresses Tbx18 and Islet1 transcription factors, after which expression of the Shox2 and Tbx3 transcription factors is initiated and that of Nkx2.5 is down-regulated [14,24,25]. RT-PCR analysis of non-differentiated MDSCs (Fig. 2a, Supplementary Table 1) revealed that Tbx18, Islet1, Shox2 and Tbx3 were expressed, whereas Nkx2.5 was not. Notably, Shox2 is a core component of the myogenic program resulting in development of the venous pole and pacemaker [25], and also of the pacemaker program in embryoid bodies [26]. Pacemaker-like differentiated MDSC-PMs likewise expressed Tbx18, Tbx3 and Islet1 no longer expressed Shox2 and showed little or no expression of Nkx2.5. This specific expression pattern is consistent with the identification of beating myocytes differentiated *in vitro* from MDSCs as mature cardiac pacemaker myocytes and not fetal-derived immature cardiomyocytes. Indeed, pacemaker cells in the adult heart differ from atrial and ventricular cardiomyocytes in that they do not express Nkx2.5, which acts as a repressor of the pacemaker gene expression program [14,25]. In addition, pacemaker myocytes are unique in retaining Islet1 expression in adult heart [27].

A hallmark of cardiac pacemaker cells is their expression of the channel HCN4 [28], which is responsible for generating the "funny" current (I_f) [29]. RT-PCR analysis of pacemaker-like MDSC-PMs (Fig. 2b, Table S1) showed that they express the pore-forming subunits of HCN4 and $Ca_V1.3$ channels, both of which are required for normal cardiac pacemaker activity in mice [30-34] and humans [35,36]. MDSC-PMs also express the pacemaker-specific gap junction protein Cx45 [14,37] and the cardiac contractile proteins α-actinin and Troponin I (Fig. 2b). The co-expression of these

proteins in beating pacemaker-like cells was tested by double-immunofluorescence of cultured, differentiated MDSCs, with cells undergoing sustained beating filmed before fixation. Fig. 2c shows immunostaining of MDSC-PMs for HCN4 and $Ca_v1.3$. Given that HCN proteins, $Ca_v1.3$, and Cx45 are also markers of neural cells, co-staining for cytoskeletal markers of striated muscle cells (cardiac Troponin I or sarcomeric α-actinin) was necessary to confirm the cardiac phenotype (Fig.2c). Of note, in the panels showing co-staining for α-actinin and Cx45, a typical neural cell on the right expressed Cx45 but not α-actinin. Fig. 2d displays cells co-stained for $Ca_v1.3$ and Islet1 (nuclei indicated by arrows including a phase-contrast field showing that both markers are expressed in beating cells (see Supplementary video 4).

Importantly, *in vitro* differentiation of muscle-derived stem cells into MDSC-PMs was not a peculiarity of mouse muscle stem cells. It was also observed in muscle stem cells isolated from adult Sprague Dawley rat muscle (Supplementary Fig. 2 and Supplementary video 5), and both the kinetics and co-expression of pacemaker markers (shown in Fig.S2 are HCN4 and α-Actinin) were similar to that in mice.

We next tested MDSC-PMs for the functional properties of native sino-atrial pacemaker using current-clamp recordings (Fig. 3). Readings from isolated beating pacemaker-like myocytes revealed spontaneous repetitive action potentials at rates comparable to those produced by native SAN pacemaker myocytes (170 bpm in pacemaker-like myocytes, Fig. 3a, versus 190 bpm in native SAN myocytes [33]). Consistent with HCN4-positive staining (Fig.2), MDSC-PM myocytes displayed the I_f current (Fig. 3b), which is involved in the pacemaker activity of native SAN myocytes [29,38]. We then recorded the spontaneous contraction frequency of beating cells by using a cell edge detection device (see methods). The selective I_f inhibitor ivabradine (IVA) [39] reduced the frequency of spontaneous cell contraction by more than 75%, demonstrating that the I_f is a key determinant of the spontaneous activity of pacemaker-like myocytes (Fig. 3c).

Whether contracting myocytes generate spontaneous intracellular Ca^{2+} ($[Ca^{2+}]_i$) transients similar to those produced by native mouse sino-atrial pacemaker myocytes was tested by loading MSDC-PMs with Fluo-4-AM. Line-scan images (Fig. 3d) revealed spontaneous $[Ca^{2+}]_i$ transients with upstroke and recovery phases similar in form and timing to those of native mouse pacemaker myocytes [34,40,41]. Line-scan images were recorded before and after the cultures were perfused with epinephrine or acetylcholine, to determine whether the frequency of spontaneous $[Ca^{2+}]_i$ transients was regulated in opposite directions by the activation of β-adrenergic [34] and muscarinic [42] receptors. Indeed, epinephrine (2 nM, Fig. 3d) accelerated, whereas acetylcholine (50 nM, Fig. 3d) reduced, the frequency of spontaneous $[Ca^{2+}]_i$ transients. Ryanodine receptors (RyRs) are also involved in sino-atrial pacemaker activity (reviewed in ref. [43]) and perfusion of MSDC-PMs with ryanodine (3

μM, Fig. 3d) led to a near-complete arrest of spontaneous $[Ca^{2+}]_i$ transients. Thus, RyRs appear to play a major role in the automaticity of MDSC-PMs, similar to that in native SAN pacemakers [43].

We previously showed that loss of $Ca_V1.3$ channels slows automaticity and leads to arrhythmia in native SAN myocytes [30,34]. To test whether MDSC-PMs differentiated from $Ca_V1.3$ knockout ($Ca_V1.3^{-/-}$) mice reproduced the phenotype of native $Ca_V1.3^{-/-}$ SAN myocytes, we compared their beating frequency to that of MDSC-PMs derived from wild-type MDSCs. As shown Fig. 3e, the rate of spontaneous $[Ca^{2+}]_i$ transients in MDSC-PMs differentiated from $Ca_V1.3^{-/-}$ MDSCs was significantly slower and their frequency less regular than those in MDSC-PMs from wild type MDSCs, consistent with findings from our previous work on native SAN myocytes from $Ca_V1.3^{-/-}$ mice [34,42].

Together, these data show that MDSCs are capable of differentiating, *in vitro*, into beating pacemaker-like myocytes with all the specific markers and electrophysiological properties of native cardiac pacemaker cells. Furthermore, *in vitro* differentiation of MDSCs derived from the muscle of bradycardic SND $Ca_V1.3^{-/-}$ mutant reproduced the slower beating phenotype of bradycardic SND $Ca_V1.3^{-/-}$ mutant hearts. These results also demonstrate that $Ca_V1.3$ channels play a key role in the pacemaker activity of MDSC-PMs, consistent with *in vivo* data from $Ca_V1.3^{-/-}$ mice [42,44,45] and from humans carrying congenital loss-of-function of $Ca_V1.3$ channels [36].

***In vivo* analysis: MDSCs injected into mice lacking $Ca_V1.3$ and $Ca_V3.1$ channels migrate and home to the SAN where they differentiate resulting in improved heart rate**

To test the ability of MDSCs to differentiate *in vivo* into pacemaker cells and their potential therapeutic effects, we employed the $Ca_V1.3^{-/-}$ deficient mouse, a well-characterized model of human SAN dysfunction [36,42], as recipients in stem cell transplantation experiments. Both embryonic stem cells (ESCs) and induced pluripotent stem cells (iPSC) can be differentiated into SAN-like cardiomyocytes *in vitro* and have been shown to provide promising short-term "biological" pacemaker activity in the ventricle [46-49]. However, the high proliferation rate and associated tumorigenicity of these cell types preclude their direct use as stem cells for *in vivo* cell therapy in the absence of previous differentiation. In contrast, we found no evidence for a long-term teratogenic or tumorigenic potential of MDSCs (Supplementary Fig. 3a). Whereas mouse ESCs grafted subcutaneously onto 8-week-old immunodeficient SCID mice (n=2) induced tumour outgrowth at the site of the graft, requiring euthanasia after 3 weeks, no tumours formed in mice (n=4) engrafted with MDSCs, and the animals remained tumour-free for over 4 months after either sub-cutaneous (Supplementary Fig. 3a) or intraperitoneal transplantation (data not shown, n=6). In addition, RT-PCR analysis (n=4) revealed that MDSCs express 3 of 4 pluripotency transcription factors (Sox2, Nanog, Lin28) but not the major one, Pou5F1/Oct4 (Supplementary Fig. 3b) a result

confirmed by RNAseq analysis on triplicate MDSC samples. The lack of teratoma formation after MDSC injection supports the direct use of these stem cells *in vivo*, without the need for prior differentiation.

At 24 and 72 hours after I.V. injection, DiI membrane-labelled MDSCs were found to be similarly distributed to major filtration organs (e.g., liver and kidney) and lymph organs (spleen and lymph nodes) in wild-type and mutant recipient mice (Davaze, Mitutsova et al. manuscript in preparation). Similar analyses of I.P.-injected, labelled-MDSCs showed enhanced MDSC homing to organs with targeted injury, such as streptozotocin-damaged pancreatic islets [50]. Thus, MDSCs used directly as stem cells *in vivo* without prior differentiation have the ability to migrate and home to a variety of organs. This property was exploited to test the capacity of MDSCs to migrate to the SAN tissue, differentiate *in vivo,* and restore compromised heart automaticity in our mouse models with SAN-dysfunction, as represented in Fig.4a. MDSCs labelled with the membrane-binding cell tracker DiI-CM were transplanted, by I.V. or I.P. injection, into $Ca_v1.3^{-/-}$ mutant mice with severe defects in SAN impulse generation and atrioventricular conduction as well as into age-matched wild-type counterparts. At 48 hours after injection, a significant number of labelled stem cells were found implanted in the SAN tissue of recipient $Ca_v1.3^{-/-}$ mice (Fig.4c), whereas only few were present in the SAN of wild-type mice (Fig.4b); this finding was reproduced in 4 wild-type and 4 $Ca_v1.3^{-/-}$ mutant mice using the same MDSC preparation. These results show that in the $Ca_v1.3^{-/-}$ mutant mouse, effective migration of stem cells into the bloodstream after I.P. injection occurred and engraftment to the SAN tissue was enhanced compared to that in wild type SAN tissue. Such increased homing of MDSCs in mutant SAN tissue may be related to the SDF-1–CXCR4 chemotactic axis, a major pathway in the regulation of stem-cell migration and homing [51,52]. Indeed, comparison of the expression of SDF1 and CXCR4 levels in SAN tissue isolated from the two groups of mice showed that SAN tissue from $Ca_v1.3^{-/-}$ mice expressed higher levels of both SDF1 and CXCR4 than did SAN tissue from wild-type counterparts (RT-PCR analysis in Supplementary Fig. 4).

To determine whether SAN engraftment of injected wild type MDSC was followed by their differentiation into cardiac myocytes, we isolated intact SAN tissue from the hearts of $Ca_v1.3^{-/-}$ mice 30 to 40 days after MDSC injection and performed whole-mount immunostaining for cells expressing the $Ca_v1.3$ pore-forming $\alpha 1$ subunit, which is absent from SAN tissue originating from the recipient mutant mouse [44,53]. As shown Fig.5, the SAN of transplanted $Ca_v1.3^{-/-}$ mice was positive for $Ca_v1.3$ staining. Notably, arrays of cells (zoomed panels 5a and 5c with 49 and 54 $Ca_v1.3$ -expressing cells, respectively) showed membrane and striated patterns of staining for $Ca_v1.3$ similar to those for native mouse SAN pacemaker cells [53], including increased staining at junctions between cells with typical pacemaker morphology (arrow in Fig. 5b).

The effectiveness of the differentiation of MDSCs into $Ca_v1.3$-expressing myocytes and their long-term colonisation was further confirmed by clear detection of $Ca_v1.3$-stained cells in the SAN of $Ca_v1.3^{-/-}/Ca_v3.1^{-/-}$ double-mutant mice 5 months after IV injection of wild-type MDSCs (Supplementary Fig. 5). Staining for $Ca_v1.3$ was specific because it was absent in the SAN of control mock-transplanted $Ca_v1.3^{-/-}$ mice (n=5, Supplementary Fig. 6).

Whether colonization of the SAN by MDSCs and their differentiation in bradycardic mutant mice was accompanied by an improvement in heart rhythm was determined by analyzing heart rate during the resting (daylight) period. To this end, telemetric ECG recordings were made in freely moving $Ca_v1.3^{-/-}$ mice, before and at different times after the injection of undifferentiated wild-type MDSCs (Fig. 6a). Consistent with a previous study [44], $Ca_v1.3^{-/-}$ mice experienced SAN dysfunction and atrioventricular blocks before injection, (Fig. 6a and Table 1). However, by 40 days after systemic transplantation of muscle-derived stem cells, the MDSC-injected mice had a significantly higher (32%, Fig. 6b) heart rate than before the procedure (Fig. 6b and Table 1), indicating that the SAN pacemaker activity had improved. Heart rate elevation in $Ca_v1.3^{-/-}$ mice was due to improvement of SAN rate (PP interval). No significant differences were observed in heart rate and the other ECG parameters in wild-type mice. Similarly, no significant changes in heart rate were observed following implantation of only a ECG transmitter (no MDSCs; Supplementary Fig. 7a) or when control wild-type mice were injected with MDSCs (Table 1). All control animals were kept under identical conditions as MDSC-injected $Ca_v1.3^{-/-}$ mice. Measurement of QT, rate-corrected QT (QTc) and QRS ECG intervals showed that MDSC injection did not affect ventricular repolarization, and no episodes of ventricular arrhythmia or sudden death were observed in MDSC-injected $Ca_v1.3^{-/-}$ and wild-type mice (Table 1). We then tested whether injection of MDSC could improve the heart rate in mice lacking both $Ca_v1.3$ and $Ca_v3.1$ channels ($Ca_v1.3^{-/-}/Ca_v3.1^{-/-}$)[54]. This mouse model presents with strong SND hallmarks and highly variable SAN rate. If MDSC injection ameliorated the heart rate of $Ca_v1.3^{-/-}/Ca_v3.1^{-/-}$ mice, this would have been reflected as an increase in SAN rate and in a reduction in the inter beat variability. Indeed, upon injection of wild-type MDSCs, the heart rates of $Ca_v1.3^{-/-}/Ca_v3.1^{-/-}$ mice were clearly improved within 30 days (as measured during the active night-time period: +20%) (Fig. 6c-d, Table 2). Heart rate of double-mutant $Ca_v1.3^{-/-}/Ca_v3.1^{-/-}$ and wild-type mice was also recorded under anesthesia 10 to 20 days after injection of MDSCs. This recording of sedated mice revealed a significant increase in heart rate in the double-mutant mice by 10 days (+28%, Supplementary Fig. 7b) and a decrease in the inter beat standard deviation after 20 days (Supplementary Fig. 7c), whereas similar injection of MDSCs into wild-type mice did not result in significant changes in either heart rate or inter beat standard deviation (Supplementary Fig. 7b-c). The number of SAN pauses or AV blocks after MDSC injection into either single $Ca_v1.3^{-/-}$ or double $Ca_v1.3^{-/-}/Ca_v3.1^{-/-}$ mutants did not change significantly (Table 1 and

2). Together these data show that systemic injection of wild-type MDSCs into bradycardic mutant mice resulted in a significant improvement in the heart rate of mutant mice whereas it did not affect the heart rate of wild-type mice.

Discussion

Our data reveal that skeletal muscle harbours a population of non-tumorigenic stem cells, MDSC, that can be directly transplanted by systemic injection and are capable of differentiating into functional pacemaker-like myocytes. Given the limitations of other sources that have been considered, MDSCs represent an attractive and easily available source of stem cells with a high potential for use in cell therapy for the treatment of disorders of human heart automaticity.

In the last decade, human myoblasts (derived from satellite cells) have been on early clinical trial as a source of stem cells for myocardial autologous cell therapy raising hope of bringing functional benefit (reviewed by Menasché [55]). However, it is now clearly recognized that myoblasts do not differentiate into cardiomyocytes after injection into the heart, but instead may fuse into multinucleated myotubes. Such differentiation may cause conduction blocks eventually leading to ventricular arrhythmia. This disappointing outcome essentially put a brake on considering skeletal muscle as a source of stem cells in cardiac cell therapy. Although most of the regenerative capacity of skeletal muscle throughout life is accounted for by satellite cells, it has become clear that the muscle niche is remodelled in dynamic balance with other stem cells derived from peri-vascular and peri-neural muscle compartment that represent an alternative source of MDSCs [2,9,10].

Taking into account this alternative, our study opens a new avenue of research on the use of skeletal muscle as a source of stem cells in therapies for diseases of heart automaticity. Indeed, our data show that the systematic injection of undifferentiated MDSCs produced functional improvements in heart rhythm (and reduced arrhythmia) in recipient mutant mice, with the stem cells migrating and homing to the SAN region and differentiating into pacemaker-like cells expressing the $Ca_v1.3$ channel. Whereas alternative approaches towards effective biological pacing have been reported, with some using ion channel gene transfer in the ventricular conduction system [22,56] and others *in situ* reprogramming of ventricular cardiomyocytes [57], the current study is the first to demonstrate direct repair of the SAN through the *in situ* differentiation of transplanted stem cells. Although transplantation of a similar population of MDSCs has been reported to improve recovery of the heart from ischemic injury, the effect in that case was attributed to the secretion of paracrine factors without significant retrieval or differentiation of donor stem cells [58]. ESCs and iPSCs can differentiate into beating, pacemaker-like cells *in vitro* [46,47]. These differentiated cells were recently shown to be able to engraft in the ventricle and support pacemaker activity [48,49]. However, their transforming and teratoma-forming potential precludes their direct use for cell therapy and requires

prior cueing toward cardiac differentiation, with a potential loss of plasticity, migration and survival ability [46,59]. In contrast, MDSCs, which are non-tumorigenic, were directly transplanted into the bloodstream or peritoneal space of mutant recipient mice, where they not only homed to the SAN and differentiated into beating, pacemaker-like cells, but also reduced defects in heart automaticity that are associated with the knock-out of the $Ca_V1.3$ Ca^{2+} channel [44]. Importantly, we also show here that MDSCs can differentiate *in vitro* into spontaneously active MDSC-PMs, displaying features of mature SAN pacemaker cells. This also make MDSCs a convenient source of stem cells to recapitulate defects in heart automaticity ex vivo and assay potential therapeutic drugs.

In SAN cells, heart automaticity is generated by an association between the activity of ion channels such as $Ca_V1.3$ [30], HCN4 [38] and that of RyR-dependent Ca^{2+} release from the sarcoplasmic reticulum [43]. Genetic ablation (from muscle-donor mouse) or pharmacologic inhibition of these channel activities in spontaneously active MDSC-PMs reproduced slowing of pacemaker activity, as reported in the current literature on native SAN-resident pacemaker cells. Our results thus indicate that the pacemaker mechanism underlying spontaneous activity of MDSC-PMs is similar to that of native SAN, and support the notion that MDSCs differentiated *in vitro* from mutant mice can reproduce and model heart-rhythm dysfunctions. This hypothesis is in line with the capability of MDSCs to improve the heart rate of mutant mice following their colonization of the SAN and differentiation at this site.

Although the mechanism underlying the spontaneous ability of MDSCs to migrate and home to the SAN tissue of mutant mice is not fully understood, it likely involves chemotaxis via the SDF1-CXCR4 pathway, as supported by data shown in Supplementary Fig. 4. Furthermore, in light of reports on heart regeneration by exercise-activated cardiac stem cells [60], on the activation of muscle stem cells by exercise (review by Macaluso & Myburgh [61]), and on the presence of stem cells from recipient patients in transplanted human hearts (i.e., “chimeric transplanted hearts”) [62,63], it is tempting to speculate that some stem cells that have been classified as "resident cardiac” may have originated from exercise-activated circulating MDSCs. It is known that denervation, like exercise, results in long-lasting activation and proliferation of resident muscle stem cells but that 90% of these cells are subsequently lost from the muscle (and not fused to the denervated-re-innervated muscle) [64]. In this regard, it will be important to compare profiles of circulating stem cells retrieved after exercise or muscle denervation to those in the resting state.

We recently showed that the MDSCs studied here migrate and home to streptozotocin-damaged pancreatic islets 48 hours after I.P. injection and that within 10 days they differentiate into cells expressing insulin [50]. Further, we found that MDSCs are recruited to site(s) of injury, be it chemically induced [50] or mechanically induced (such as glycerol injection in one of the two tibialis

muscles) (Davaze, Mitutsova et al., manuscript in preparation). Thus, the capability of MDSCs to migrate and home to damaged tissues could be exploited for therapeutic purposes.

SAN dysfunction is a multi-factorial disease that often begins with a moderate reduction in heart rate that is otherwise asymptomatic, and that this subsequently degenerates into bradycardia associated with invalidating symptoms and syncope [65]. Early therapy of SAN dysfunction could potentially avoid or delay the need to implant an electronic pacemaker [20]. In this regard, restoring damaged or degenerated SAN tissue by direct transplantation of MDSCs, in particular from the own muscle of the patient, constitutes an attractive possibility. We found that amelioration of heart rate in bradycardic mice occurs about 3 weeks following cell transplantation. This delay presumably reflects the time required for MDSCs to differentiate into MDSC-PMs. However, we recently also showed that the inhibition of G-protein gated K^+ channels (I_{KACh}) (by either genetic deletion or a pharmacologic agent) may rescue the SAN dysfunction and heart block normally observed in $Ca_V1.3^{-/-}$ mice [42]. It is thus possible that future therapies for SAN dysfunction may combine a pharmacologic strategy such as I_{KACh} inhibtion to improve heart rate in the short term, followed by a long-term cell therapy-based approach employing MDSCs.

Materials and Methods

Mouse strains

Six to ten week-old wild-type C57Bl/6 mice or transgenic C57Bl/6 "green mice" expressing eGFP under beta-actin promoter[66] were used to prepare MDSC as donor mice for transplantation experiments. Recipient wild-type, $Ca_V1.3^{-/-}$ and $Ca_V1.3^{-/-}/Ca_V3.1^{-/-}$ mice used for transplantation experiments were all of C57Bl/6 genetic background [54]. All procedures were performed in accordance with the animal care guidelines of the European Union, French laws and the Ethical committee of the University of Montpellier (N°: 2017010310594939).

Cell culture

MDSC were prepared using the preplate procedure originally described by Qu-Petersen et al.[11] as modified in Arsic et al. [10]

Briefly, mouse hind-limb muscles were removed, minced and enzymatically dissociated at 37°C for 45 min in 0.2% collagenase A (Roche) and 1 mg/ml dispase (GibcoBRL). After digestion, muscle cells were passed through 100 µm then 40 µm nylon cell strainers (BD Falcon) and centrifuged at 360 g for 10 min. Pelleted cells were washed twice in phosphate buffer saline (PBS), suspended in growth medium GM [DMEM/F12 (SIGMA, Les Ulis, France), 16% fetal bovine serum (PAA), 1% Ultroser G (Pall Life Sciences, Washington, USA), 100uM Beta-mercapto-ethanol, antibiotic-antimycotic mix (Gibco, Invitrogen Inc. Saint Quentin Fallavier, France) and plated on uncoated

dishes (NUNC). After an initial 40 min pre-plating, non-adherent cells were collected and transferred to a new dish. The same operation was repeated every 24 h for 7 days with the addition of a centrifugation step at 360g, followed by resuspending the pelleted non-adherent cells in fresh GM.

MDSC used for RNA extraction, I.V. and I.P. transplantation and sub-cutaneous grafting experiments were non-adherent cells obtained after 6-7 days sequential pre-plating of stem cells extracted from hind limb skeletal muscle of adult mice.

Mouse adult fibroblast (MAF) were obtained from ATCC (Ltk-11) and grown as recommended by the supplier. Mouse ESCs were grown and harvested as described[67].

Immunofluorescence analysis

Immunofluorescence analysis was performed on 2-6 week-cultured differentiated MDSC obtained from serial preplates as described[10]. Cells were fixed with 3.7% formaldehyde for 5 min, snap permeabilized for 30 sec in -20°C acetone, preincubated 30 min with 0.5% BSA in PBS. Cells were then incubated for 1h at 37°C with primary antibodies against HCN4, (1:100, Alomone), sarcomeric α-actinin, clone EA-53 (1:100, Sigma-Aldrich), connexin45 (1:100, H-85, Santa Cruz Biotechnology), $Ca_V1.3$ polyclonal antibody[53], cardiac troponin I (1:100, Millipore), Islet1 monoclonal antibody 39.3f7 (developed by Thomas M. Jessell and Susan Brenner-Morton and obtained from the Developmental Studies Hybridoma Bank, created by the NICHD of the NIH and maintained at The University of Iowa, Department of Biology, Iowa City, IA 52242). Specific staining was revealed using anti-mouse or anti-rabbit Alexa Fluor 488 and Alexa Fluor 555-conjugated secondary antibodies (InVitrogen) with Hoechst33358 nuclear stain (0.1 µg/ml) for 30 min at 37°C.

RNA isolation and reverse transcription polymerase chain reaction

Total RNA was extracted from sino-atrial node tissue, ventricular tissue, ESCs, mouse adult fibroblasts, MDSC and *in vitro* cultured differentiated MDSC using RNeasy kit (Qiagen) and then treated with RQ1 DNase treatement (Promega) according to the manufacturer's recommendations. Ventricular and sino-atrial node tissues were obtained from 7-week-old C57Bl/6 adult male mice. Total RNA was used to synthesize cDNA using the Superscript III reverse transcriptase kit (Invitrogen) with random primers or with gene-specific primer in the case of Hcn4. The gene specific primers for Hcn4, were designed from alignment of four sequences (Hcn1, Hcn2, Hcn3 and Hcn4) and chosen on the basis of a specific N-terminal Hcn4 fragment. PCR was performed with GoTaq DNA polymerase (Promega); primer sequences are shown in supplemental Table S1. The cDNA was amplified using 35 cycles of PCR with an annealing temperature of 60°C to 62°C. PCR

products were separated on 2% agarose gel (Invitrogen), stained with ethidium bromide; visualized and photographed on a UV transluminator (Fischer Scientific). For comparative RNA expression in whole muscle cells from first preplate: PP1 (at 24h) versus the 8th preplate: PP8-MDSC shown Fig.1b: data shown are from pseudo-counts-RLE obtained after RNAseq analysis of triplicate samples from RNA banks made with the TruSeq Stranded mRNA sample preparation kit (Illumina) and sequencing with a HiSeq2500 Illumina sequencer (MGX Montpellier GenomiX: http://www.mgx.cnrs.fr)

Cell transplantation experiments

Intravenous (I.V.) and intraperitoneal (I.P.) transplantation experiments were performed using wild-type, $Ca_v1.3^{-/-}$ or $Ca_v1.3^{-/-}/Ca_v3.1^{-/-}$ mice as recipients. MDSC were extracted from wild-type C57Bl/6 or transgenic C57Bl/6 mice expressing eGFP under the control of a beta-actin promoter[66]. Approximately $5x10^5$ cells per recipient mouse were resuspended in 0.9% sodium chloride solution and injected into the tail vein. Mock-transplanted $Ca_v1.3^{-/-}$ mice were injected with sodium chloride solution alone. Transplanted mice were sacrificed 2, 10, 20, 30 and 41 days after injection followed by sino-atrial node dissection. For cell tracking experiments in the SAN tissue, MDSC were labelled before injection for 30 min with the lipophilic membrane-bound cell tracker DiI-CM (C7000 at 1μg/ml, ThermoFisher Scientific) according to the manufacturer's instruction.

Immunohistochemistry

Sino-atrial node tissue was dissected and fixed in 4% formaldehyde for 20 min before washing in PBS. After permeabilization in -20°C acetone, the whole SAN tissue was rehydrated with PBS. Non-specific binding of antibodies was blocked by incubation for 1h at room temperature with blocking solution (10% goat serum (Abcam), 0.1% Triton X-100 in PBS) followed by incubation with Mouse Ig Blocking Reagent (Vector Laboratories) for 30 min. Permeabilized and blocked sino-atrial tissue was then incubated overnight at 4°C with primary polyclonal anti-$Ca_v1.3$-α1 subunit antibodies (prepared as described in ref. [53] ,1:500) diluted in 1% goat serum in PBS. Alexa488 or 555 fluorochrome goat anti-rabbit secondary antibodies (1:100, InVitrogen) in 1% goat serum were applied for 30 min at 37°C with Hoechst33358 nuclear stain (0.1 μg/ml) for 40 min at 37°C. Autofluorescence was quenched by incubating in 1% Sudan Black B (Sigma-Aldrich) in 70% ethanol for 10 min before washing in 70% ethanol for 5 min at room temperature. Tissues were mounted with AirVol mounting medium before photomicroscopy as described in Arsic et al.[10]. The specificity of $Ca_v1.3$ staining was confirmed by its absence in sino-atrial tissue prepared from non-injected $Ca_v1.3^{-/-}$ mice.

Measurements of contraction frequency

Cellular contraction of differentiated MDSC-PM was measured by an edge-detection IonOptix system device (LLC, 309 Hillside Street, Milton, MA 02186, USA). Cells were grown in 35 mm dishes in complete medium and analysed on an Olympus IX71 inverted microscope. MDSC-PM were imaged at 120 Hz using an IonOptix™ Myocam-S CCD camera. Digitized images were displayed within the IonWizard™ acquisition software (IonOptix™). To measure changes in cell length, two cursors were placed at opposing edges of the cell defined as difference in optical density (maximum: dark; minimum: light). The relative movement of cursors assessed cell shortening. Experiments were performed at 36 °C.

Electrophysiological recordings of beating MDSC-PM, differentiated from MDSC in vitro

For electrophysiological recordings, aliquots of the cell suspension were harvested in custom made recording chambers (working volume 500 µL) allowing controlled unidirectional solution flow and mounted on the stage of an Olympus, X71 inverted microscope, and continuously perfused with normal Tyrode solution. The recording temperature was set to 36°C. The whole-cell variation of the patch-clamp technique[68] was used to record cellular ionic currents, employing an Axopatch 200A (Axon Instruments Inc., Foster USA) patch-clamp amplifier, grounded by an agar bridge filled with 150 mM KCl. Cellular automaticity was recorded by the perforated patch technique with escin (50 µM). Recording electrodes were pulled from borosilicate glass, using a Flaming-Brown microelectrode puller (Sutter, Novato CA, USA). For recording cell automaticity, as well as I_f we used an intracellular solution containing (mM/L): K^+-aspartate, 130; NaCl, 10; ATP-Na^+ salt, 2; creatine phosphate, 6.6; GTP-Mg^{2+}, 0.1; $CaCl_2$, 0.04 (pCa=7); Hepes-KOH, 10; (adjusted to pH=7.2 with KOH). Electrodes had a resistance of about 5 MΩ. Seal resistances were in the range of 2-5 GΩ. The extracellular solution contained (in mM/L): NaCl, 140; KCl, 5.4; $CaCl_2$, 1.8; $MgCl_2$, 1; Hepes-NaOH, 5; and D-glucose, 5.5; (adjusted to pH=7.4 with NaOH). I_f was routinely recorded in Tyrode solution containing 5 mM $BaCl_2$ to block I_{K1}. Data was acquired with pClamp software (ver. 9, Axon Instruments Inc.).

Confocal imaging of $[Ca^{2+}]_i$ transients and measurements of contraction.

Intracellular Ca^{2+} ($[Ca^{2+}]_i$) transients were imaged by loading *in vitro* differentiated MDSC-PM with the Ca^{2+} indicator Fluo-4 AM 15 µM (from a stock solution in a mixture of DMSO/Pluronic F-127) in the medium for 45 min at 37°C. Spontaneous $[Ca^{2+}]_i$ transients were recorded in differentiated pulsing MDSC-PM loaded with Fluo-4 AM under control conditions

(culture medium), or medium containing either epinephrine, acetylcholine (ACh) or ryanodine. Recordings were performed at 36°C. Differentiated MDSC-PM were distinguished from other cell types (i.e. fibroblasts and adipocytes cells) by their morphology (spindle and elongated shape), size (~10 μm diameter) and pulsing activity. Extended Datavideos S1-S3 show examples of differentiated MDSC-PM with typical morphology.

$[Ca^{2+}]_i$ transient images were obtained by confocal microscopy (Meta Zeiss LSM 510 and Zeiss LSM 780) scanning cells with an Argon laser in line scan configuration (1.54 ms line rate); fluorescence was excited at 488 nm and emissions collected at >505 nm. A 63x water immersion objective (n.a. 1.2), a 63x oil immersion objective (n.a. 1.32) and a 40x objective (n,a. 1.2) were used for recordings in differentiated pulsing MDSC-PM. Image analyses were performed using ImageJ software. Images were corrected for background fluorescence and the fluorescence values (F) normalized to basal fluorescence (F_0) in order to obtain the fluorescence ratio (F/F_0). Light intensity intervals were analyzed by pClamp software (ver. 9, Axon Instruments Inc.).

Microscope and video imaging system

Digital images were collected using Leica DM LB microscope and Canon EOS300D digital camera as described before[10]. Videos of contracting cells were recorded using a NIKON D90 camera coupled to a Zeiss Axiovert 35M. A Nanozoomer Hamamatsu blade scanner was used for 2D reconstruction of whole mount SAN tissue (in Fig. S5 and Fig. S6).

Tumour formation assay

$1x10^6$ MDSC resuspended in 0.2 ml of 1/2X matrigel in HBSS were injected subcutaneously into the back of n=4 8-week-old SCID/beige mice (Charles River). Follow up observation was carried out for up to 4 months.

ESCs derived tumours were obtained by similar subcutaneous injection of $1x10^6$ mouse ESCs into the back of 8-week-old SCID/beige mice (n=2). Tumours developed in all ES-grafted mice within 2 weeks. The mice were euthanized after 4 weeks when tumour size reached more than 2 cm.

ECG recordings and analysis in sedated mice

One-lead surface ECG measurements were recorded from wild-type and $Ca_v1.3^{-/-}/Ca_v3.1^{-/-}$ mice sedated with 1.5% isofluorane. Body temperature was continuously maintained at 36° -37°C using a heated pad connected to a controller that received feedback from a temperature sensor attached to the mouse. Ag/AgCl gel-coated ECG electrodes (Unomedical) were attached to the superior right and both inferior limbs of mice. The electrodes were connected to a standard one-lead ECG amplifier module (EMKA Technologies, Paris, France), which included high- and low-pass

filters (set to 0.05 Hz and 500 Hz, respectively) and a gain selection device (set to 1,000-fold). Signals were digitized continuously at 2 kHz and recorded using an IOX data acquisition system (EMKA Technologies, France). The recordings were carried out for a 45-min period before (day 0) and at different days after transplantation (day 10 and day 20). The software ecgAuto (EMKA Technologies, France) was used to perform offline analysis of the data recorded. For each mouse the mean heart rate value and the Standard Deviation (SD) were calculated. Beat-to-beat analysis of heart rate was carried out on a 30-min interval taken 10 min after the beginning of each 45-min recording.

Telemetric recordings of ECG and analysis

For telemetric ECG recording, adult wild-type and $Ca_V1.3^{-/-}$ male mice were anesthetized with 2% isofluorane. A midline incision was made on the back along the spine to insert a telemetric transmitter (TA10EA-F20, Data Sciences International) into a subcutaneous pocket with paired wire electrodes placed over the thorax (chest bipolar ECG lead). Local anaesthesia was obtained with lidocaine (1%) injected subcutaneously at the sites of electrodes and transmitter implantation. To manage possible post-surgery pain, Advil (paracetamol and ibuprofene, 7 mL/l) was added to the drinking water for four days after implantation. Mice were housed in individual cages with free access to food and water and were exposed to 24-hour light/dark cycles (light, 8:30 AM to 8:30 AM) in a thermostatically controlled room. Heart rates were averaged over a 24-hour recording period or over two 12-hour periods corresponding to "day-time" (light, 8:30 AM to 8.30 PM) or "night-time" (dark, 8.30 PM to 8.30 AM). Recordings were initiated at least 8 days after recovery from surgical implantation. ECG signals were recorded using a telemetry receiver and an analog-to-digital conversion data acquisition system for display and analysis by DataquestTM A.R.T.TM software (Data Sciences International). ECG parameters were measured using ecgAuto 1.5.7 software. RR, PR, QRS, QT and QTc intervals were first calculated automatically by ecgAuto based on a large (>250) ECG sample library and then verified by visual inspection. Heart rates (in bpm) were then determined from RR intervals. PP intervals were measured manually over shorter recording windows.

Statistical analysis

The statistical significance of measured differences in heart rates or cellular rates of contraction was evaluated through paired or unpaired Student's t test. Statistical significance was set at $p<0.05$. Data analysis was performed with GraphPad Prism 6.0

Author Contributions

A.F. and M.E.M. designed and analysed the experiments. P.M., D.M., I.B. performed the experiments with additional input from A.G.T., V.M., R.D., M.L.D.F., N.A., J.N., A.L. and N.J.C.; D.M. performed muscle stem cell culture and differentiation, RT-PCR analysis with advice from N.A. and immunocyto- and histochemistry with supervision from A.F. and N.J.L.; P.M. performed whole-cell patch clamp, Ca^{2+} imaging and ECG telemetric recordings with supervision from M.E.M.; J.S. provided research tools; A.F. and M.E.M wrote the manuscript with comments and approval from all co-authors.

Acknowledgements

We thank Chantal Jacquet (IGMM, Montpellier) for initial help with MDSC I.V. injection, MRI and RHEM from Biocampus Montpellier facilities, Dr. Olivier Ganier (IGH) for mouse embryonic stem cells and Dr. G Enikolopov (Cold Spring Harbor Laboratory, NY, USA) for the transgenic mouse line Nestin-eGFP described in Mignone et al. 2004. The hybridoma monoclonal antibodies Nestin (Rat-401) developed by S. Hockfield, and Islet1 39.3f7 developed by Thomas M. Jessell and Susan Brenner-Morton were obtained from the Developmental Studies Hybridoma Bank, created by the NICHD of the NIH and maintained at The University of Iowa, Department of Biology, Iowa City, IA 52242.

Funding.

P.M. and A.G.T. were supported by a Research Training Network (RTN) "CavNet" funded through the EU Research Programme (6FP) MRTN-CT-2006-035367. The IGF group is a member of the Laboratory of Excellence “Ion Channel Science and Therapeutics” supported by a grant from ANR (ANR-11-LABX-0015). D.M. and V.M. were supported by Association Francaise contre les Myopathies (AFM). Research supported by the Fondation pour la Recherche Medicale "Physiopathologie Cardiovasculaire" (DPC20111122986 to A.F.), by Agence Nationale de Recherche (ANR-2010-BLAN-1128-01 to MEM and AF), NIH (DC009433, HL087120 to A.L.), University of Iowa Carver Research Program of Excellence Award (to A.L.), the Austrian Science Fund (F27809 to J.S.).

References

1 Peault, B. *et al.* Stem and progenitor cells in skeletal muscle development, maintenance, and therapy. *Mol Ther* **15**, 867-877, doi:6300145 [pii] 10.1038/mt.sj.6300145 (2007).

2 Tamaki, T. Bridging long gap peripheral nerve injury using skeletal muscle-derived

multipotent stem cells. *Neural Regen Res* **9**, 1333-1336, doi:10.4103/1673-5374.137582 (2014).

3 Tamaki, T., Uchiyama, Y. & Akatsuka, A. Plasticity and physiological role of stem cells derived from skeletal muscle interstitium: contribution to muscle fiber hyperplasia and therapeutic use. *Curr Pharm Des* **16**, 956-967 (2010).

4 Yin, H., Price, F. & Rudnicki, M. A. Satellite cells and the muscle stem cell niche. *Physiol Rev* **93**, 23-67, doi:10.1152/physrev.00043.2011 (2013).

5 Ten Broek, R. W., Grefte, S. & Von den Hoff, J. W. Regulatory factors and cell populations involved in skeletal muscle regeneration. *J Cell Physiol* **224**, 7-16, doi:10.1002/jcp.22127 (2010).

6 Romero-Ramos, M. *et al.* Neuronal differentiation of stem cells isolated from adult muscle. *J Neurosci Res* **69**, 894-907, doi:10.1002/jnr.10374 (2002).

7 Alessandri, G. *et al.* Isolation and culture of human muscle-derived stem cells able to differentiate into myogenic and neurogenic cell lineages. *Lancet* **364**, 1872-1883, doi:S0140-6736(04)17443-6 [pii] 10.1016/S0140-6736(04)17443-6 (2004).

8 Uezumi, A. *et al.* Functional heterogeneity of side population cells in skeletal muscle. *Biochem Biophys Res Commun* **341**, 864-873, doi:S0006-291X(06)00104-5 [pii] 10.1016/j.bbrc.2006.01.037 (2006).

9 Tamaki, T. *et al.* Clonal multipotency of skeletal muscle-derived stem cells between mesodermal and ectodermal lineage. *Stem Cells* **25**, 2283-2290, doi:10.1634/stemcells.2006-0746 (2007).

10 Arsic, N., Mamaeva, D., Lamb, N. J. & Fernandez, A. Muscle-derived stem cells isolated as non-adherent population give rise to cardiac, skeletal muscle and neural lineages. *Exp Cell Res* **314**, 1266-1280, doi:S0014-4827(08)00019-0 [pii] 10.1016/j.yexcr.2008.01.009 (2008).

11 Qu-Petersen, Z. *et al.* Identification of a novel population of muscle stem cells in mice: potential for muscle regeneration. *J Cell Biol* **157**, 851-864, doi:10.1083/jcb.200108150 jcb.200108150 [pii] (2002).

12 Gharaibeh, B. *et al.* Isolation of a slowly adhering cell fraction containing stem cells from murine skeletal muscle by the preplate technique. *Nat Protoc* **3**, 1501-1509, doi:nprot.2008.142 [pii] 10.1038/nprot.2008.142 (2008).

13 Mangoni, M. E. & Nargeot, J. Genesis and regulation of the heart automaticity. *Physiol Rev* **88**, 919-982 (2008).

14 Christoffels, V. M., Smits, G. J., Kispert, A. & Moorman, A. F. Development of the pacemaker tissues of the heart. *Circ Res* **106**, 240-254, doi:106/2/240 [pii] 10.1161/CIRCRESAHA.109.205419 (2010).

15 Wiese, C. *et al.* Formation of the sinus node head and differentiation of sinus node myocardium are independently regulated by Tbx18 and Tbx3. *Circ Res* **104**, 388-397, doi:CIRCRESAHA.108.187062 [pii] 10.1161/CIRCRESAHA.108.187062 (2009).

16 Verheijck, E. E., Wilders, R. & Bouman, L. N. Atrio-sinus interaction demonstrated by blockade of the rapid delayed rectifier current. *Circulation* **105**, 880-885 (2002).

17 Watanabe, E. I. *et al.* Modulation of pacemaker activity of sinoatrial node cells by electrical load imposed by an atrial cell model. *Am J Physiol* **269**, H1735-1742 (1995).

18 Verheule, S. & Kaese, S. Connexin diversity in the heart: insights from transgenic mouse models. *Front Pharmacol* **4**, 81, doi:10.3389/fphar.2013.00081 (2013).

19 Mesirca, P., Torrente, A. G. & Mangoni, M. E. Functional role of voltage gated Ca(2+) channels in heart automaticity. *Front Physiol* **6**, 19, doi:10.3389/fphys.2015.00019 (2015).

20 Jensen, P. N. *et al.* Incidence of and risk factors for sick sinus syndrome in the general population. *J Am Coll Cardiol* **64**, 531-538, doi:S0735-1097(14)02843-5 [pii] 10.1016/j.jacc.2014.03.056 (2014).

21 Mond, H. G. & Proclemer, A. The 11th world survey of cardiac pacing and implantable cardioverter-defibrillators: calendar year 2009--a World Society of Arrhythmia's project. *Pacing Clin Electrophysiol* **34**, 1013-1027, doi:10.1111/j.1540-8159.2011.03150.x (2011).

22 Rosen, M. R., Robinson, R. B., Brink, P. R. & Cohen, I. S. The road to biological pacing. *Nat Rev Cardiol* **8**, 656-666, doi:nrcardio.2011.120 [pii] 10.1038/nrcardio.2011.120 (2011).

23 Besson, V. *et al.* PW1 gene/paternally expressed gene 3 (PW1/Peg3) identifies multiple adult stem and progenitor cell populations. *Proc Natl Acad Sci U S A* **108**, 11470-11475, doi:10.1073/pnas.1103873108 (2011).

24 Hoogaars, W. M. *et al.* Tbx3 controls the sinoatrial node gene program and imposes pacemaker function on the atria. *Genes Dev* **21**, 1098-1112 (2007).

25 Ye, W. *et al.* A common Shox2-Nkx2-5 antagonistic mechanism primes the pacemaker cell fate in the pulmonary vein myocardium and sinoatrial node. *Development* **142**, 2521-2532, doi:10.1242/dev.120220 (2015).

26 Hashem, S. I. *et al.* Shox2 regulates the pacemaker gene program in embryoid bodies. *Stem Cells Dev* **22**, 2915-2926, doi:10.1089/scd.2013.0123 (2013).

27 Weinberger, F. *et al.* Localization of Islet-1-positive cells in the healthy and infarcted adult murine heart. *Circ Res* **110**, 1303-1310, doi:CIRCRESAHA.111.259630 [pii] 10.1161/CIRCRESAHA.111.259630 (2012).

28 Ludwig, A., Zong, X., Jeglitsch, M., Hofmann, F. & Biel, M. A family of hyperpolarization-activated mammalian cation channels. *Nature* **393**, 587-591 (1998).

29 Brown, H. F., DiFrancesco, D. & Noble, S. J. How does adrenaline accelerate the heart? *Nature* **280**, 235-236 (1979).

30 Mangoni, M. E. *et al.* Functional role of L-type Cav1.3 Ca2+ channels in cardiac pacemaker activity. *Proc Natl Acad Sci U S A* **100**, 5543-5548 (2003).

31 Alig, J. *et al.* Control of heart rate by cAMP sensitivity of HCN channels. *Proc Natl Acad Sci U S A* **106**, 12189-12194 (2009).

32 Baruscotti, M. *et al.* Deep bradycardia and heart block caused by inducible cardiac-specific knockout of the pacemaker channel gene Hcn4. *Proc Natl Acad Sci U S A* **108**, 1705-1710, doi:1010122108 [pii] 10.1073/pnas.1010122108 (2011).

33 Mesirca, P. *et al.* Cardiac arrhythmia induced by genetic silencing of 'funny' (f) channels is rescued by GIRK4 inactivation. *Nat Commun* **5**, 4664, doi:ncomms5664 [pii] 10.1038/ncomms5664 (2014).

34 Torrente, A. G. *et al.* L-type Cav1.3 channels regulate ryanodine receptor-dependent Ca2+ release during sino-atrial node pacemaker activity. *Cardiovasc Res* **109**, 451-461, doi:cvw006 [pii] 10.1093/cvr/cvw006 (2016).

35 Milanesi, R., Baruscotti, M., Gnecchi-Ruscone, T. & DiFrancesco, D. Familial sinus bradycardia associated with a mutation in the cardiac pacemaker channel. *N Engl J Med* **354**, 151-157 (2006).

36 Baig, S. M. *et al.* Loss of Ca(v)1.3 (CACNA1D) function in a human channelopathy with bradycardia and congenital deafness. *Nat Neurosci* **14**, 77-84, doi:nn.2694 [pii] 10.1038/nn.2694 (2011).

37 Verheijck, E. E. *et al.* Electrophysiological features of the mouse sinoatrial node in relation to connexin distribution. *Cardiovasc Res* **52**, 40-50 (2001).

38 DiFrancesco, D. The role of the funny current in pacemaker activity. *Circ Res* **106**, 434-446, doi:106/3/434 [pii] 10.1161/CIRCRESAHA.109.208041 (2010).

39 Bois, P., Bescond, J., Renaudon, B. & Lenfant, J. Mode of action of bradycardic agent, S 16257, on ionic currents of rabbit sinoatrial node cells. *Br J Pharmacol* **118**, 1051-1057 (1996).

40 Sah, R. *et al.* Ion channel-kinase TRPM7 is required for maintaining cardiac automaticity. *Proc Natl Acad Sci U S A* **110**, E3037-3046, doi:1311865110 [pii] 10.1073/pnas.1311865110 (2013).

41 Chen, B., Wu, Y., Mohler, P. J., Anderson, M. E. & Song, L. S. Local control of Ca2+-induced Ca2+ release in mouse sinoatrial node cells. *J Mol Cell Cardiol* **47**, 706-715, doi:S0022-2828(09)00276-4 [pii] 10.1016/j.yjmcc.2009.07.007 (2009).

42 Mesirca, P. *et al.* G protein-gated IKACh channels as therapeutic targets for treatment of

sick sinus syndrome and heart block. *Proc Natl Acad Sci U S A* **113**, E932-941, doi:1517181113 [pii] 10.1073/pnas.1517181113 (2016).

43 Lakatta, E. G., Maltsev, V. A. & Vinogradova, T. M. A coupled SYSTEM of intracellular Ca2+ clocks and surface membrane voltage clocks controls the timekeeping mechanism of the heart's pacemaker. *Circ Res* **106**, 659-673, doi:106/4/659 [pii] 10.1161/CIRCRESAHA.109.206078 (2010).

44 Platzer, J. *et al.* Congenital deafness and sinoatrial node dysfunction in mice lacking class D L-type Ca2+ channels. *Cell* **102**, 89-97 (2000).

45 Zhang, Z. *et al.* Functional Roles of Ca(v)1.3 (alpha(1D)) calcium channel in sinoatrial nodes: insight gained using gene-targeted null mutant mice. *Circ Res* **90**, 981-987. (2002).

46 Laflamme, M. A. & Murry, C. E. Heart regeneration. *Nature* **473**, 326-335, doi:nature10147 [pii] 10.1038/nature10147 (2011).

47 Kleger, A. *et al.* Modulation of calcium-activated potassium channels induces cardiogenesis of pluripotent stem cells and enrichment of pacemaker-like cells. *Circulation* **122**, 1823-1836, doi:CIRCULATIONAHA.110.971721 [pii] 10.1161/CIRCULATIONAHA.110.971721 (2010).

48 Chauveau, S. *et al.* Induced Pluripotent Stem Cell-Derived Cardiomyocytes Provide In Vivo Biological Pacemaker Function. *Circ Arrhythm Electrophysiol* **10**, e004508, doi:CIRCEP.116.004508 [pii] 10.1161/CIRCEP.116.004508 (2017).

49 Protze, S. I. *et al.* Sinoatrial node cardiomyocytes derived from human pluripotent cells function as a biological pacemaker. *Nat Biotechnol* **35**, 56-68, doi:10.1038/nbt.3745 (2017).

50 Mitutsova, V. *et al.* Adult muscle-derived stem cells engraft and differentiate into insulin-expressing cells in pancreatic islets of diabetic mice. *Stem Cell Res Ther* **8**, 86, doi:10.1186/s13287-017-0539-9 (2017).

51 Miller, R. J., Banisadr, G. & Bhattacharyya, B. J. CXCR4 signaling in the regulation of stem cell migration and development. *J Neuroimmunol* **198**, 31-38, doi:10.1016/j.jneuroim.2008.04.008 (2008).

52 Stumm, R. & Hollt, V. CXC chemokine receptor 4 regulates neuronal migration and axonal pathfinding in the developing nervous system: implications for neuronal regeneration in the adult brain. *J Mol Endocrinol* **38**, 377-382, doi:10.1677/JME-06-0032 (2007).

53 Christel, C. J. *et al.* Distinct localization and modulation of Cav1.2 and Cav1.3 L-type Ca2+ channels in mouse sinoatrial node. *J Physiol* **590**, 6327-6342, doi:jphysiol.2012.239954 [pii] 10.1113/jphysiol.2012.239954 (2012).

54 Marger, L. *et al.* Functional roles of Ca(v)1.3, Ca(v)3.1 and HCN channels in automaticity of mouse atrioventricular cells: insights into the atrioventricular pacemaker mechanism. *Channels (Austin)* **5**, 251-261, doi:15266 [pii] (2011).

55 Menasche, P. Stem cell therapy for chronic heart failure: lessons from a 15-year experience. *C R Biol* **334**, 489-496, doi:10.1016/j.crvi.2011.03.006 (2011).

56 Boink, G. J. *et al.* HCN2/SkM1 gene transfer into canine left bundle branch induces stable, autonomically responsive biological pacing at physiological heart rates. *J Am Coll Cardiol* **61**, 1192-1201, doi:S0735-1097(13)00182-4 [pii] 10.1016/j.jacc.2012.12.031 (2013).

57 Kapoor, N., Liang, W., Marban, E. & Cho, H. C. Direct conversion of quiescent cardiomyocytes to pacemaker cells by expression of Tbx18. *Nat Biotechnol* **31**, 54-62, doi:10.1038/nbt.2465 (2013).

58 Okada, M. *et al.* Human skeletal muscle cells with a slow adhesion rate after isolation and an enhanced stress resistance improve function of ischemic hearts. *Mol Ther* **20**, 138-145, doi:10.1038/mt.2011.229 (2012).

59 Mohsin, S., Siddiqi, S., Collins, B. & Sussman, M. A. Empowering adult stem cells for myocardial regeneration. *Circ Res* **109**, 1415-1428, doi:109/12/1415 [pii] 10.1161/CIRCRESAHA.111.243071 (2011).

60 Ellison, G. M. *et al.* Adult c-kit(pos) cardiac stem cells are necessary and sufficient for functional cardiac regeneration and repair. *Cell* **154**, 827-842 (2013).

61 Macaluso, F. & Myburgh, K. H. Current evidence that exercise can increase the number of adult stem cells. *J Muscle Res Cell Motil* **33**, 187-198, doi:10.1007/s10974-012-9302-0 (2012).

62 Quaini, F. *et al.* Chimerism of the transplanted heart. *N Engl J Med* **346**, 5-15, doi:10.1056/NEJMoa012081 (2002).

63 Laflamme, M. A., Myerson, D., Saffitz, J. E. & Murry, C. E. Evidence for cardiomyocyte repopulation by extracardiac progenitors in transplanted human hearts. *Circ Res* **90**, 634-640 (2002).

64 Murray, M. A. & Robbins, N. Cell proliferation in denervated muscle: time course, distribution and relation to disuse. *Neuroscience* **7**, 1817-1822 (1982).

65 Semelka, M., Gera, J. & Usman, S. Sick sinus syndrome: a review. *Am Fam Physician* **87**, 691-696, doi:d10507 [pii] (2013).

66 Okabe, M., Ikawa, M., Kominami, K., Nakanishi, T. & Nishimune, Y. 'Green mice' as a source of ubiquitous green cells. *FEBS Lett* **407**, 313-319, doi:S0014-5793(97)00313-X [pii] (1997).

67 Ganier, O. *et al.* Synergic reprogramming of mammalian cells by combined exposure to mitotic Xenopus egg extracts and transcription factors. *Proc Natl Acad Sci U S A* **108**, 17331-17336, doi:1100733108 [pii] 10.1073/pnas.1100733108 (2011).

68 Hamill, O. P., Marty, A., Neher, E., Sakmann, B. & Sigworth, F. J. Improved patch-clamp techniques for high-resolution current recording from cells and cell-free membrane patches. *Pflugers Archiv - European Journal of Physiology* **391**, 85-100 (1981).

Figure 1

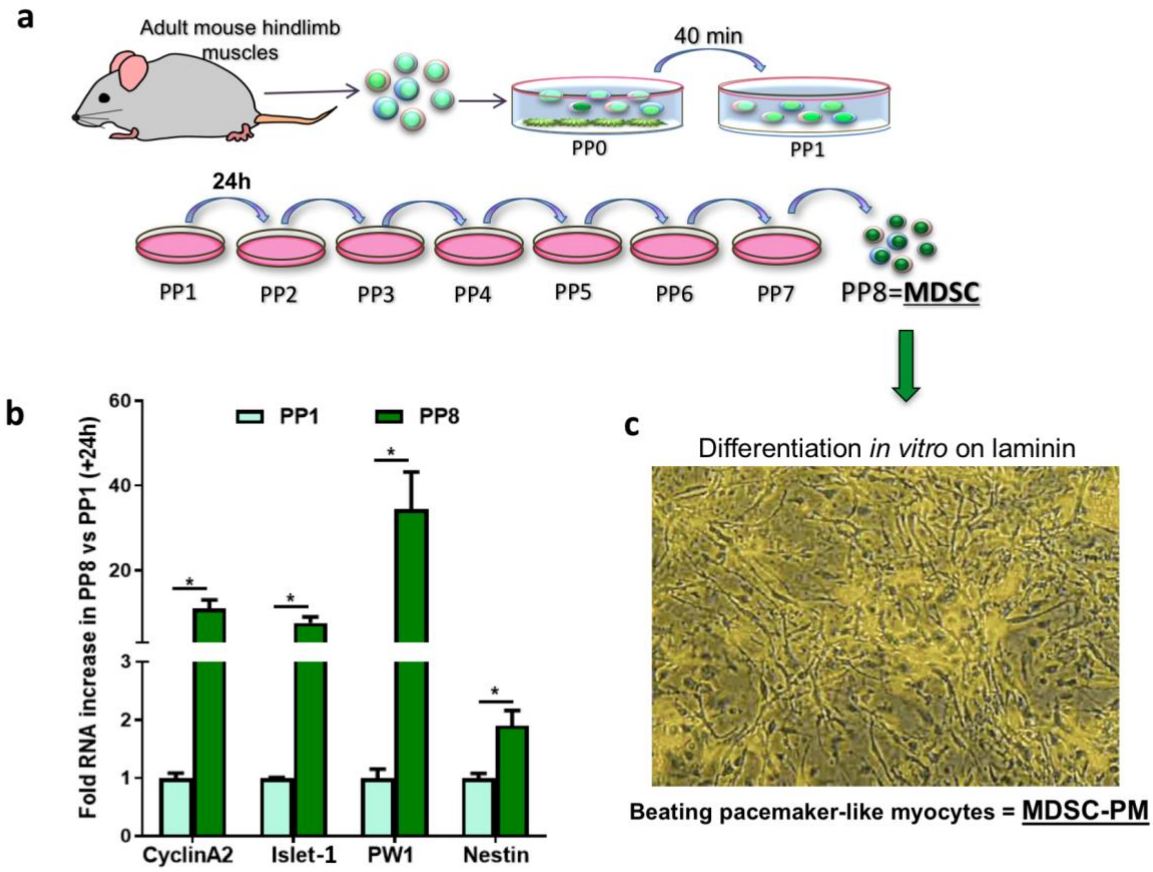

Fig 1. **Muscle stem cell isolation, expression of stemness factors, and differentiation of pacemaker-like cells *in vitro*. a:** Schematic overview of the protocol for isolating non-adherent muscle-derived stem cells (MDSCs) from mouse hind-limb muscle. **b**: Levels of RNA expression for *CyclinA2*, *Islet-1*, *Peg3/PW1,* and *Nestin* in PP1 muscle cells cultured for 24 hours versus MDSC PP8 cells, as determined by RNAseq profiling of independent replicates. Shown are the fold increase in PP8 MDSCs vs. PP1 cells (levels in PP1 cells normalized as 1x). *$p<0.05$. **c**: Phase-contrast image of MDSCs differentiated into muscle stem cell-derived pacemaker myocytes (MDSC-PMs) after 3 weeks on laminin. The field is the same as that shown in Supplementary video 1.

Figure 2

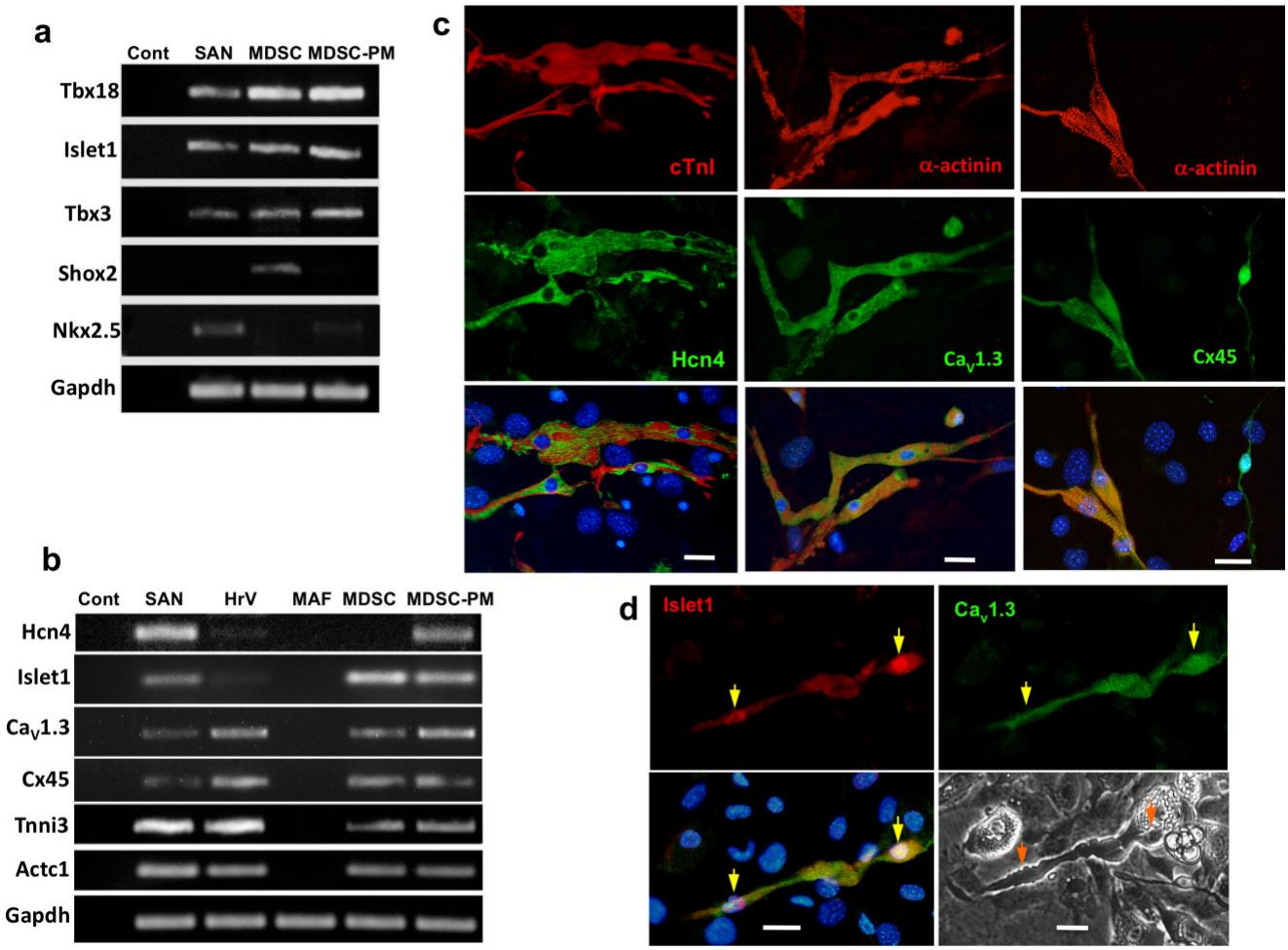

Fig 2. Expression of sino-atrial markers in MDSCs and in MDSC-PMs differentiated *in vitro* from MDSCs. a. RT-PCR-based analysis of expression of transcription factors involved in sino-atrial node (SAN) development (Tbx18, Islet1, Tbx3, Shox2 and Nkx2.5). SAN: mouse sino-atrial node; MDSCs: muscle-derived stem cell; MDSC-PMs: MDSCs differentiated *in vitro* into pacemaker-like beating cells. GAPDH was used as loading control. **b.** RT-PCR-based analysis of expression of cardiac pacemaker-specific markers in mouse. HCN4; Islet-1; Cav1.3; Cx45 (Connexin45); Tnni: (cardiac Troponin I); Actc: (cardiac α-actinin). SAN, heart ventricles (HrV); mouse adult fibroblasts (MAF). Control without cDNA are indicated as Cont. Results for (a) and (b) are representative of analysis of n=3 independent MDSC and MDSC-PM RNA preparations. **c.** Co-immunostaining of MDSC-PMs for HCN4 and cardiac TroponinI (cTnI); sarcomeric α-actinin and Cav1.3; and sarcomeric α-actinin and Connexin45 (Cx45). **d.** Co-immunostaining for Islet1 and Cav1.3, and phase-contrast image of 2 beating MDSC-PMs (indicated by arrows) that are also shown in Supplementary video S4. Immunostaining is representative of n=20 independent cultures of MDSC-PMs from wild-type mouse muscle. Scale bars, 10 μm.

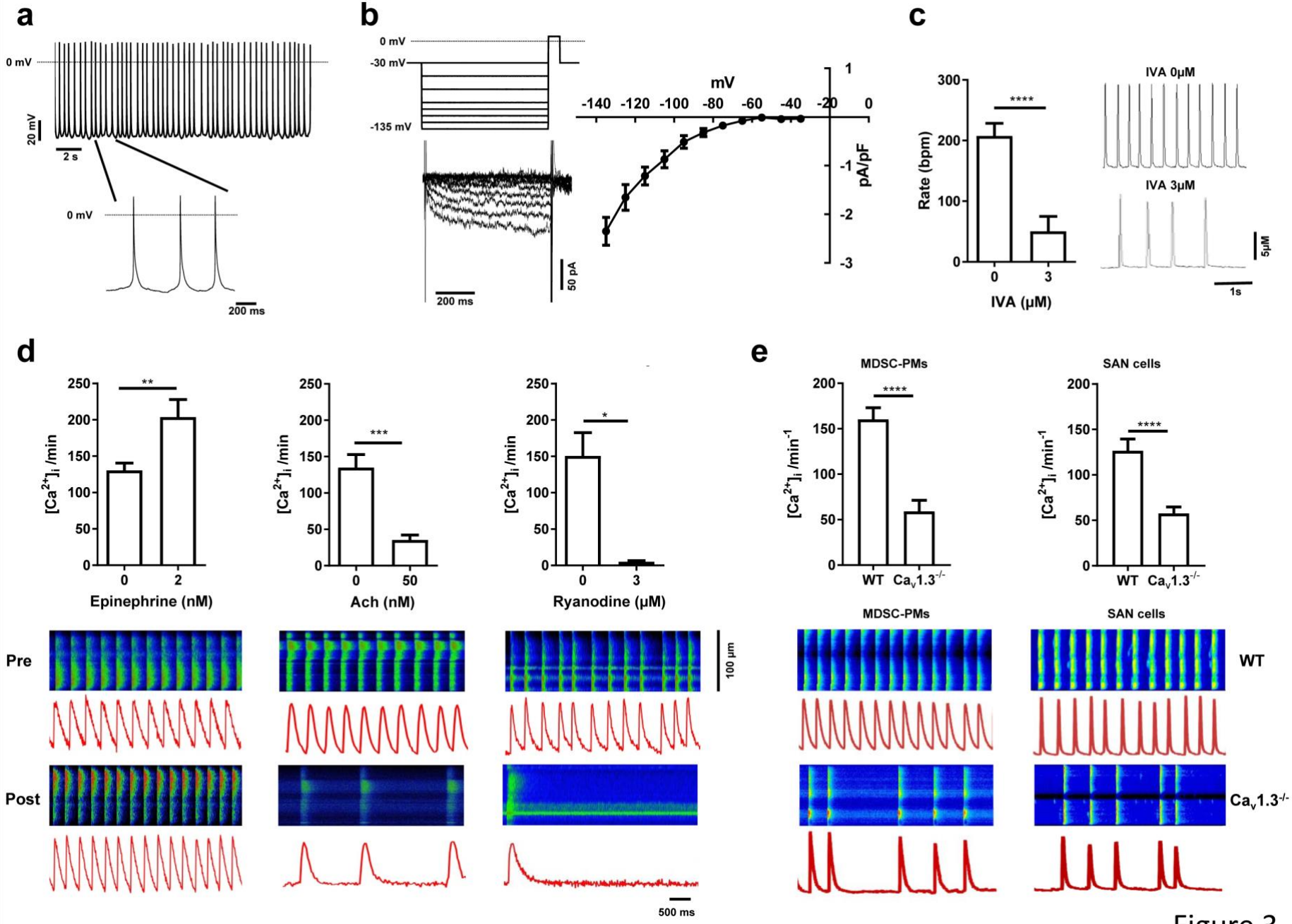

Figure 3

Fig. 3. Electrophysiology and Ca^{2+} signaling in pacemaker-like MDSC-PMs differentiated *in vitro*. a. Representative traces of action potentials recorded from *in vitro*-differentiated beating MDSC-PMs. **b.** Voltage protocol, sample current traces *(left panel)* and averaged current-to-voltage relationship of I_f (*right panel*) recorded in differentiated MDSC-PMs (peak I_f density at –135 mV: 2.5 ± 0.2 pA/pF, n=11). I_f was evoked by applying hyperpolarizing voltage steps from a holding potential of –30 mV. **c.** Spontaneous contraction rates (*right panel*) and corresponding edge-detection recording samples (*left panel*) of *in vitro*-differentiated MDSC-PMs under control conditions, without ivabradine (0 IVA) and during perfusion with ivabradine (IVA 3 μM, n=15). **d.** Chronotropic response of Fluo-4-loaded MDSC-PMs, measured as the change in frequency of spontaneous $[Ca^{2+}]_i$ transients pre- (*top line*) and post- (*bottom line*) perfusion with the following agonists: epinephrine, 2 nM (*left panel*: n=12); acetylcholine (Ach) 50 nM (*middle panel*: n=11); and ryanodine, 3 μM (*right panel*: n=5). Corresponding representative confocal line-scan images of $[Ca^{2+}]$ transients in MDSC-PMs. Light intensity integrals (red traces) are shown underneath each scan. **e.** Spontaneous $[Ca^{2+}]$ transients in MDSC-PMs (*left panel*) derived from wild-type (WT, *top line*) and $Ca_v1.3^{-/-}$ (*bottom line*) mice, compared to spontaneous $[Ca^{2+}]$ transients measured in isolated native SAN cells *(right panel)* from wild-type (*top line*) and $Ca_v1.3^{-/-}$ (*bottom line*) mice. Light intensity integrals (red traces) are shown underneath each scan. Note that the rate of spontaneous $[Ca^{2+}]_i$ transients in MDSC-PMs differentiated from $Ca_v1.3^{-/-}$ mice are slower than those in their wild-type counterparts. Means are given ± S.E.M. *p<0.05; **p<0.01; ***p<0.001; ****p<0.0001

Figure 4

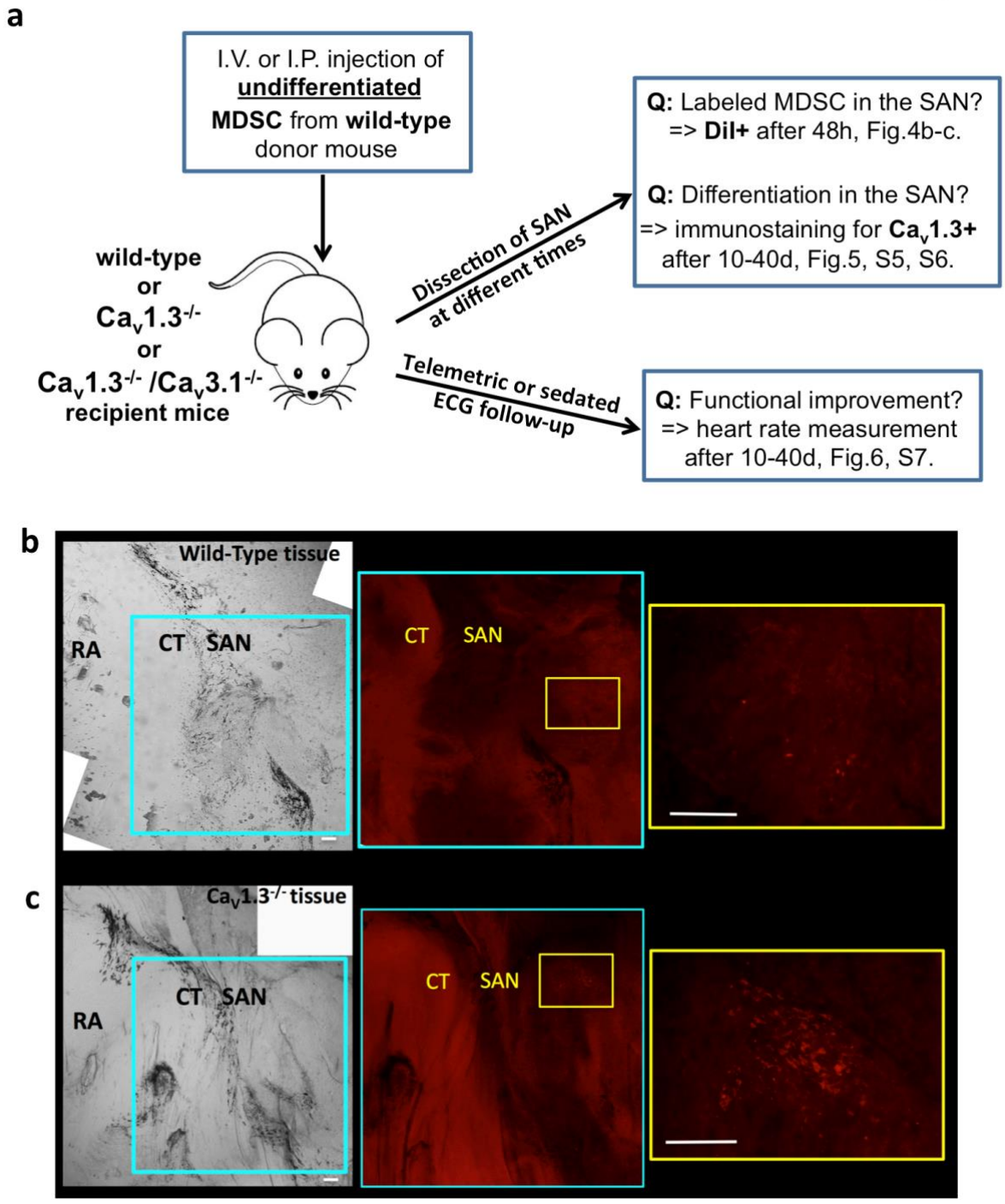

Fig. 4 Summary of *in vivo* experiments with bradycardic mutant mice and early engraftment to the SAN by MDSCs. a. Schematic representation of assays testing the reparative potential of MDSCs *in vivo*. **b-c.** Assays of MDSC migration and engraftment to SAN tissue, in age- and sex-matched wild-type and $Ca_v1.3^{-/-}$ mice 48 hours after I.P. injection with $3x10^5$ MDSCs pre-labelled with the membrane marker DiI for. **b.** SAN tissue from a male wild-type mouse injected with DiI-MDSCs. **c**. SAN tissue from a male $Ca_v1.3^{-/-}$ mouse injected with DiI-MDSCs. Shown are representative bright-field images at 60x and close-ups (areas shown by frames) of red fluorescence (DiI). RA: right atrium; CT: crista terminalis; SAN: sino-atrial node area. Bar = 200 microns.

Figure 5

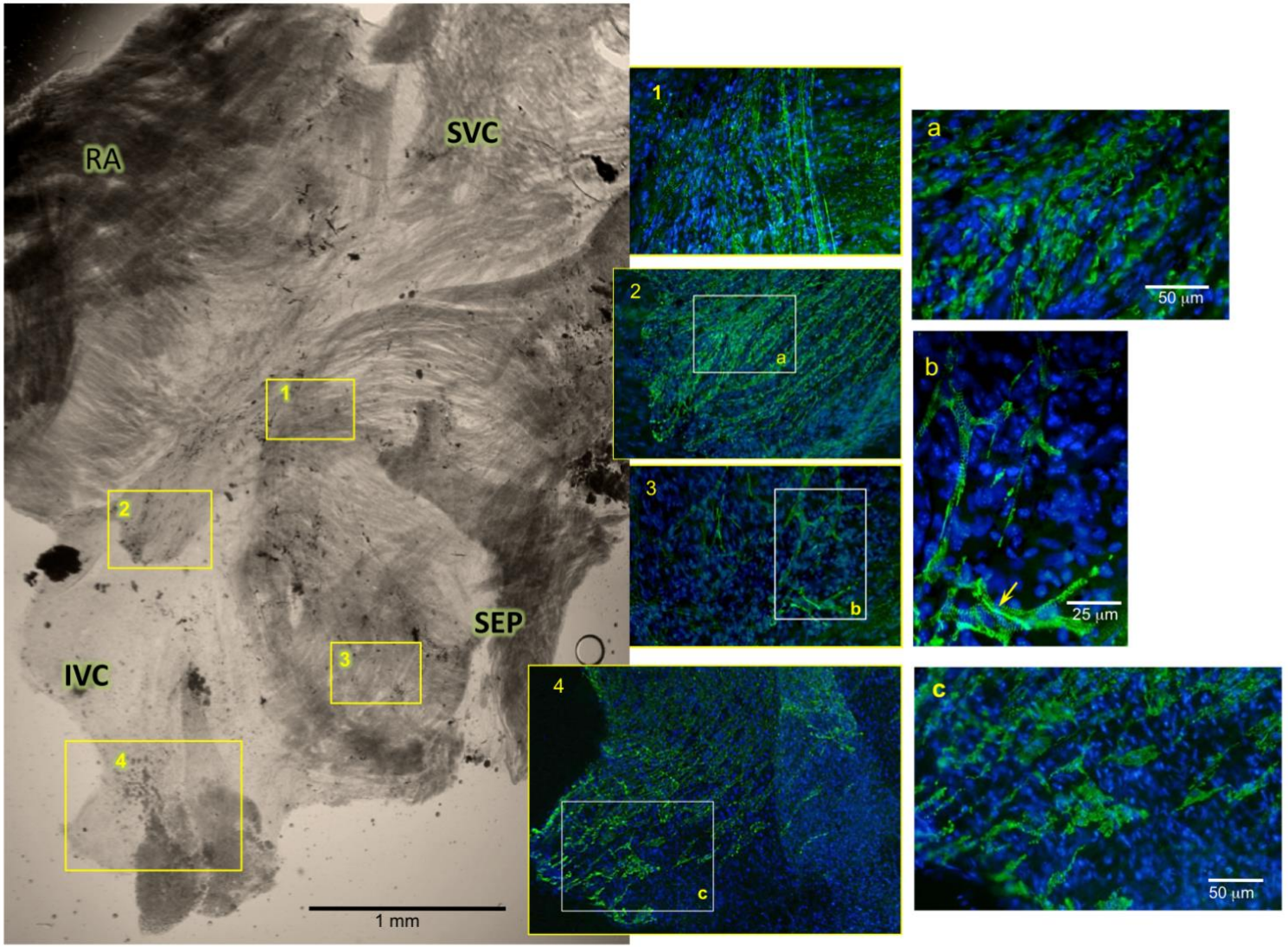

Fig. 5. Engraftment and differentiation of wild-type MDSCs in the SAN tissue of $Ca_v1.3^{-/-}$ mutant mice. SAN tissue of $Ca_v1.3^{-/-}$ mutant mice injected (I.V.) with MDSCs, shown at 40 days post-injection. Immunofluorescence labelling for $Ca_v1.3$ (green) was carried out on whole-mount SAN tissue together with Hoechst DNA staining as described in Methods. Shown are bright-field images of the whole SAN region, with the right atrium (RA, cut before final mounting), superior and inferior vena cava (SVC and IVC) and inter-atrial septum (SEP) marked. Higher-magnification immunofluorescence images of areas marked 1-4 in the bright-field image show arrays of individual $Ca_v1.3$-positive cells with typical patchy membrane staining. Further magnification of areas **a**, **b**, and **c** show membrane-associated and striated patterns, with enhanced staining at cell junctions (arrow in **b**). Similar results were obtained from 5 independent MDSC injection experiments into $Ca_v1.3^{-/-}$ mice.

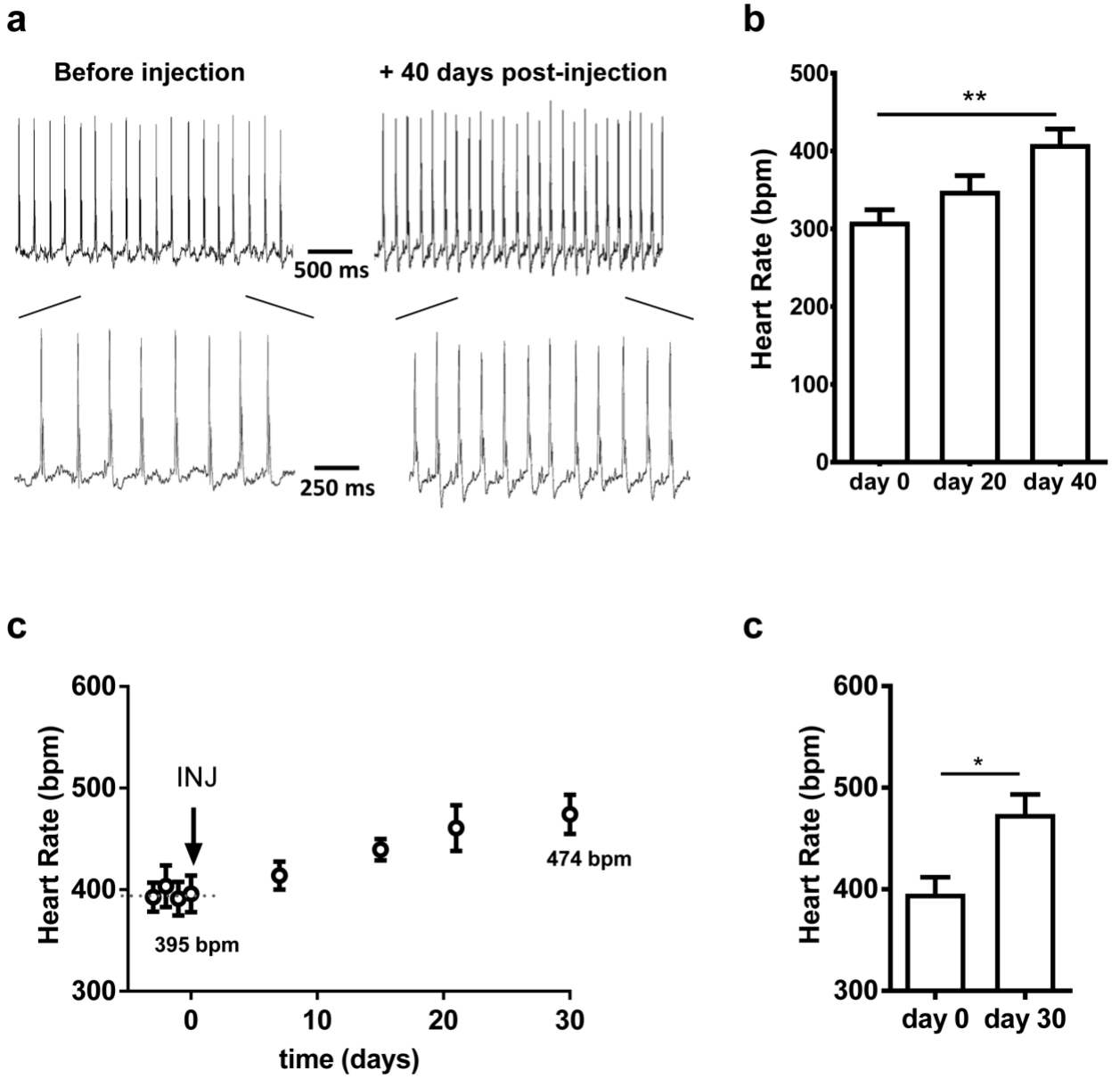

Fig. 6. *In vivo* recordings of heart rate in $Ca_v1.3^{-/-}$ single-mutant and $Ca_v1.3^{-/-}/Ca_v3.1^{-/-}$ double-mutant mice before and after transplantation of MDSCs from wild-type muscle. a. Samples of *in vivo* telemetric ECG recordings from a freely moving $Ca_v1.3^{-/-}$ mouse before and after systemic transplantation (I.V. injection) of MDSCs. **b.** Quantitation of 24-hour telemetric recordings of heart rate in n=6 $Ca_v1.3^{-/-}$ mice (see Table 1), before and up to 40 days after systemic transplantation of MDSCs. Data are presented as mean ± S.E.M. *p<0.05; **p<0.01; **c.** Quantitation of *in vivo* telemetric heart rate recordings in $Ca_v1.3^{-/-}/Ca_v3.1^{-/-}$ double mutant mice before and after systemic transplantation of MDSCs (I.P. injection). **d.** Quantitation of heart rate recorded in $Ca_v1.3^{-/-}/Ca_v3.1^{-/-}$ mice before (day 0) and on day 30 after I.P. transplantation of MDSCs from wild-type mice.

Table 1. Telemetric ECG intervals for transplanted $Ca_v1.3^{-/-}$ and wild-type mice during 12 hours resting (day) time. Shown are the values of the ECG parameters and the presence of sinus (SAN) pauses and 2nd –degree atrioventricular blocks (AVBII), (mean ± S.E.M.).

	$Ca_v1.3^{-/-}$ before injection	$Ca_v1.3^{-/-}$ 40 days post-injection	n	p value $Ca_v1.3^{-/-}$	Wild-type before injection	Wild-type 40 days post-injection	n	p value WT
Heart rate (bpm)	310 ± 15	410 ± 19	6	0.012	568 ± 6	548 ± 2	4	ns
PP (ms)	215 ± 6	169 ± 6	6	0.006	115 ± 6	112 ± 1	4	ns
PR (ms)	55 ± 2	51 ± 1	6	ns	34 ± 1	35 ± 1	4	ns
QRS (ms)	17 ± 1	16 ± 1	6	ns	10 ± 1	10 ± 1	4	ns
QT (ms)	71 ± 5	66 ± 3	6	ns	43 ± 1	41 ± 1	4	ns
QTc (ms)	50 ± 3	52 ± 2	6	ns	41 ± 1	39 ± 1	4	ns
SAN pauses/60s	0.9 ± 0.5	0.3 ± 0.1	6	ns	0	0	4	ns
AVBII/60s	0.5 ± 0.2	0.3 ± 0.1	6	ns	0	0	4	ns

Table 2. Telemetric ECG intervals for transplanted $Ca_v1.3^{-/-}/Ca_v3.1^{-/-}$ mice during 6 hours active (night) time. Summary of ECG parameters recorded in n=6 $Ca_v1.3^{-/-}/Ca_v3.1^{-/-}$ double mutant mice before (day 0) and after (day 30) 30 days following I.P. transplantation of wild-type MDSCs. Shown are the values of the ECG parameters and the presence of sinus (SAN) pauses and 2nd – degree atrioventricular blocks (AVBII), (mean ± S.E.M.).

	Day 0	Day 30	n	p value
PP (ms)	169 ± 8	135 ± 8	6	0.011
PR (ms)	54 ± 2	52 ± 1	6	ns
QRS (ms)	15 ± 1	15 ± 1	6	ns
QT (ms)	64 ± 3	62 ± 6	6	ns
QTc (ms)	50 ± 2	53 ± 4	6	ns
SAN pauses/60s	6 ± 2	2 ± 1	6	ns
AVBII/60s	6 ± 1	4 ± 2	6	ns